18 Droplet Size Distributions of Oil-in-Water Emulsions under High Pressures by Video Microscopy

Pål V. Hemmingsen, Inge H. Auflem, Øystein Sæther, and Arild Westvik

CONTENTS

18.1 INTRODUCTION

In crude oil production, gas, oil, and co-produced water are mixed due to pressure drop and high shear forces as the fluid passes the wellhead and various choke valves from the reservoir to the separation facilities. The primary task at the oil producing facility is to separate gas from liquid and oil from water. The oil and water mixture is typically processed through a separation train of two or three separators, where water is removed. The produced water contains dispersed oil droplets, which need to be removed in order to meet environmentally based, governmental demands on water quality before discharge to sea. The produced water is therefore cleaned through additional separators, cyclones, etc. before it is disposed to sea or re-injected into the reservoir.

One of the major factors influencing performance in both hydrocyclones and traditional flotation cells/plate separators is the droplet size distribution of the dispersed phase. The separation of smaller droplets is slower and more difficult. In the design and evaluation of oil–water separators in the oil industry, information concerning the sizes of droplet is critical [1]. Droplet size is an important parameter in equations describing droplet movement, such as Stokes' law for gravity induced sedimentation/creaming [2], the Stokes–Einstein equation for diffusion [3], and in equations describing sedimentation and coalescence profiles [4–6].

Samples of the produced water stream are often analyzed in a particle/droplet analyzer at the oil production facility. Such particle/droplet analyzers operate at atmospheric conditions. As the pressure of the sampled water is reduced to atmospheric pressure, dissolved gas in both the oil droplets and water may cause coalescence or re-agitation of the dispersed droplets and thereby influence the droplet size distribution. Also time will be important as the oil-in-water emulsion will not be a stable system, but will continue to separate during the time from the water sampling to the time of analysis. All these factors imply that the best way to measure the droplet size distribution is to measure it *in situ* under real conditions.

At Statoil R&D Center, development of laboratory scale high pressure separation equipment makes it possible to mix water and oil under realistic process conditions [7–9]. Connecting a video microscopy system [10] to a high pressure separation rig makes it possible to investigate the droplet distribution of emulsions at high pressures [11].

Many different techniques are used for droplet and particle size analysis: optical microscopy (photomicrography) [12,13], video microscopy [10,14–29], light scattering [30–32], electrozone sensing [1,33–35], photon correlation spectroscopy [30,36,37], turbidimetry [38–41], pulse field gradient nuclear magnetic resonance (PFG-NMR) [42–47], and ultrasonic spectroscopy [48]. Light scattering, the electrical zone sensing method, and photon correlation spectroscopy require dilution of the samples.

The different methods have different size regions which they can measure [49,50]. Not all the methods are easy to implement for measuring at high pressures. Some of the methods also need longer time for the measurement, like the PFG-NMR, which takes about 15 to 30 min, although recent advances make it possible to perform faster analyses [44]. Many of the techniques for measuring particle sizes are typically based on various forms of light scattering. The results from the light scattering techniques have to be fitted to a scattering function, where in some cases one has to assume the particle shape and also the type of size distribution (Gaussian, log–normal, etc.). These methods do not discriminate between droplets and particles.

Although optical microscopy has a long history in the determination of particle and droplet size, there has been an increase in the use of image analysis for particle and shape analysis, due to the emergence of new imaging systems and improved software. Video microscopy is a technique that combines the magnification power of a microscope with the image-acquisition capability of a video camera. The resulting data matrix, from which information about the sample can be extracted, is an image or a series of images. Current image-analysis software provides a wide range of analytical capabilities for acquiring, enhancing, and analyzing images. Video microscopy is a direct method that measures the actual size of the discrete objects. This means that multimodal size distributions will be detected properly. It also gives the shape of objects, whether or not you have multiple emulsions, and if the sample is flocculated. All the above parameters are central to the understanding of emulsion behavior and emulsion stability. Another advantage with optical microscopy, which should not be overlooked, is the fact that, as a visual image is obtained, experimental defects such as dirt covering the flow cell windows or entrapped gas bubbles can easily be detected.

18.1.1 Limitations in Video Microscopy

First, the sample must have certain optical properties, since the technique relies on reflection, refraction, scattering, and absorption of visible light. This means that the sample must be transparent and that the continuous liquid and the droplets must have different refractive indices or different colors, i.e., properties that make them optically distinguishable. Second, the resolution limit, and hence the operational size domain, is governed by the wavelength of the light. This feature is known as the Rayleigh limit and results in a physical limit of about half the illumination wavelength, i.e., 0.2 μm in the visible area.

The Rayleigh criterion [51] states that:

$$R = \frac{0.61\lambda}{\mathrm{NA}} \tag{18.1}$$

where λ is the wavelength of the light source, and NA is the numerical aperture. The numerical aperture of a microscope objective is a measure of its ability to gather light and resolve fine specimen detail at a fixed object distance. The practical limit tends to be slightly higher, 1 to 2 μm, due to rapidly increasing measurement errors with decreasing object dimensions. This is caused by diffraction: the image of an object is actually a diffraction pattern, and the overlapping patterns of closely spaced objects result in image blurring. When it comes to magnification, there is no theoretical upper limit, although increasing the magnification only renders larger, blurred images of the objects. Still, innovations in the optics have proved that the diffraction-imposed barrier is not absolute, and may be an important tool in the near future of microscopy.

For size measurements there is also a limit of how concentrated the emulsion can be, due to overlap of the droplets. A maximum droplet concentration of 1 vol% is often referred to. This is in the order of 10,000 ppm, which, in the oil production, is considered as highly polluted water, and which by no means could be disposed of without thorough cleaning. Normally, at the outlet of the first stage production separator, the amount of oil in the water varies from above 1000 ppm down to 100 ppm depending on the field conditions and the stability of the oil-in-water emulsion. The separated water then needs to be cleaned further until it meets governmental demands before it is disposed of. In the Norwegian sector of the North Sea, the maximum allowed oil content in produced water disposed to the sea is 40 ppm (in 2004), but it is proposed that the maximum is reduced to 30 ppm from the end of 2005. In this region, video microscopy should be ideal for measuring the oil droplets, with no need for dilution. Video microscopy attached to a high-pressure flow cell could then be used for online monitoring of the quality of the produced water at various stages in the water treatment process.

In this chapter we present and discuss a video microscopy system for measuring the droplet size distributions in separated water from mixed crude oil/water emulsions at realistic process conditions, i.e., at elevated temperatures and pressures.

18.2 THEORY

18.2.1 Droplet Size Distribution

Due to the high industrial importance of measuring sizes of particles as part of the manufacturing of powders, most of the theory of size measurements is based on the measuring of particles and not of droplets. However, what applies to particles with regard to size measurements and size distributions will also apply to droplets. In many cases, the term "diameter" would be well

representative of the size of spherical droplets, while particles tend to be more irregular in shape and thus the meaning of "diameter" may be interpreted differently. However, although single droplets dispersed in a diluted emulsion would be spherical, there might be some degree of flocculation, which would give clusters of droplets with irregular shape and different diameters depending on what direction it is measured.

The reporting of droplet size and droplet size distribution can be done in various forms and with various techniques [52] and it is often related to the property (number, surface area, or volume) important for the given emulsion. If the different amount of the particles/droplets is important, then the number mean diameter and number distribution should be used. This might be used in a process where one of the quality parameters is that the size of the particles should be between 10 and 20 μm, for example.

In other cases, like in the investigation of a catalyst or the amount of surfactants at the droplet interface in an emulsion, parameters describing the surface area are important. In produced water in the oil industry, the total amount of the oil in the water is important, so one should relate the diameters to the mass or volume of the dispersed oil droplets.

18.2.2 Average Diameters

The purpose of an average is to represent a group of individual values in a simple and concise manner in order to obtain an understanding of the group. It is therefore important that the average should be representative of the group. All averages are a measure of central tendency. The mean, $\overline{D}$, describes the center of gravity of the distribution [53]:

$$\overline{D} = \frac{\sum D_i \mathrm{d}\phi}{\sum \mathrm{d}\phi} \tag{18.2}$$

where ϕ is a given property.

For a number distribution $\mathrm{d}\phi = \mathrm{d}N$, giving the mean diameter as:

$$D\,(1,0) = \frac{\sum D_i \mathrm{d}N}{\sum \mathrm{d}N} \tag{18.3}$$

For a mass or volume distribution $\mathrm{d}\phi = \mathrm{dV} = D_i^3 \mathrm{d}N$, giving the volume moment mean diameter:

$$D\,(4,3) = \frac{\sum D_i^4 \mathrm{d}N}{\sum D_i^3 \mathrm{d}N} \tag{18.4}$$

18.2.3 Droplet Shape

For particles, the shape is a fundamental powder property affecting powder packing and properties like bulk density, porosity, and so on. For image analysis of droplets, the shape parameters can be used to discriminate objects that differ too much compared to a spherical shape. It can also be used to investigate the degree of flocculation, as flocculated clusters of droplets will have a different shape to that of a spherical droplet. The shape of a droplet can be described in many ways; the three used in this work are roundness, aspect, and radius ratio. The roundness is

given by:

$$\text{roundness} = \frac{P^2}{4\pi A} \tag{18.5}$$

where P is the perimeter of the droplet, and A its area. The aspect shape factor reports the ratio between the major and the minor axis of the ellipse equivalent of the object (i.e., an ellipse with the same area). The radius ratio shape factor describes the ratio between the maximum and minimum radius of each object. For a perfectly round sphere, all these parameters are equal to 1.

Combining these shape parameters, we can define an overall droplet shape factor, SF:

$$\text{SF} = \sqrt{\frac{\text{roundness}^2 + \text{aspect}^2 + \text{radius ratio}^2}{3}} \tag{18.6}$$

For a perfect sphere, the droplet shape factor defined in Equation 18.6 is equal to 1.

18.3 EXPERIMENTAL

18.3.1 Sample Preparation

Live crude oil samples and produced water were received from different North Sea oil fields. The crude oil and produced water samples were typically sampled from the outlet of the inlet production separator. The fluids were kept under pressure from field to laboratory. In order to simulate the separation in the inlet production separator, the fluids should meet the temperature and pressure conditions at the choke valve before the inlet production separator. In order to meet these fluid conditions, the crude oil samples were first heated to the elevated temperature. Any free water left in the sample was removed and the crude oil was recombined with a natural gas mixture to obtain the pressure condition at the oil field prior to the inlet production separator. The produced water samples were only heated to the experimental temperature, but not recombined with the natural gas mixture, as water has very limited solubility of natural gases.

18.3.2 High-Pressure Separation Rig

The separation rig was used to mix water and oil at elevated temperature and pressure and to monitor the subsequent separation of the phases. Figure 18.1 shows an outline of the whole rig.

The principle of the rig is that water and oil meet at elevated pressure in a pipeline and flow through a choke valve into the separation cell. The rig has three choke valves (P10, P12, and P13), giving the possibility to mix the oil and water far from the separator, in order to achieve coalescence effects in the pipeline to the separator, or to mix oil and water close to the separator. It is also possible to study the mixing of two different fluid systems by mixing each system on both sides (using choke valves P10 and P13) and then combine them at choke valve P12. The low-pressure side of choke valve P12 equals the separator pressure. The pressure drop over the choke valves provides the shear forces necessary for the mixing of water and oil and depending on the water cut one obtains a water-in-oil or oil-in-water emulsion. At the same time the light end of the oil undergoes a phase transition from liquid to gas. The gas evolved may cause foam and may influence the sedimentation and coalescence of the dispersed droplets. The separation cell is filled with a constant liquid flow for a given time. The amount of the different phases (foam, oil, emulsion layer, and water) is recorded as a function of time.

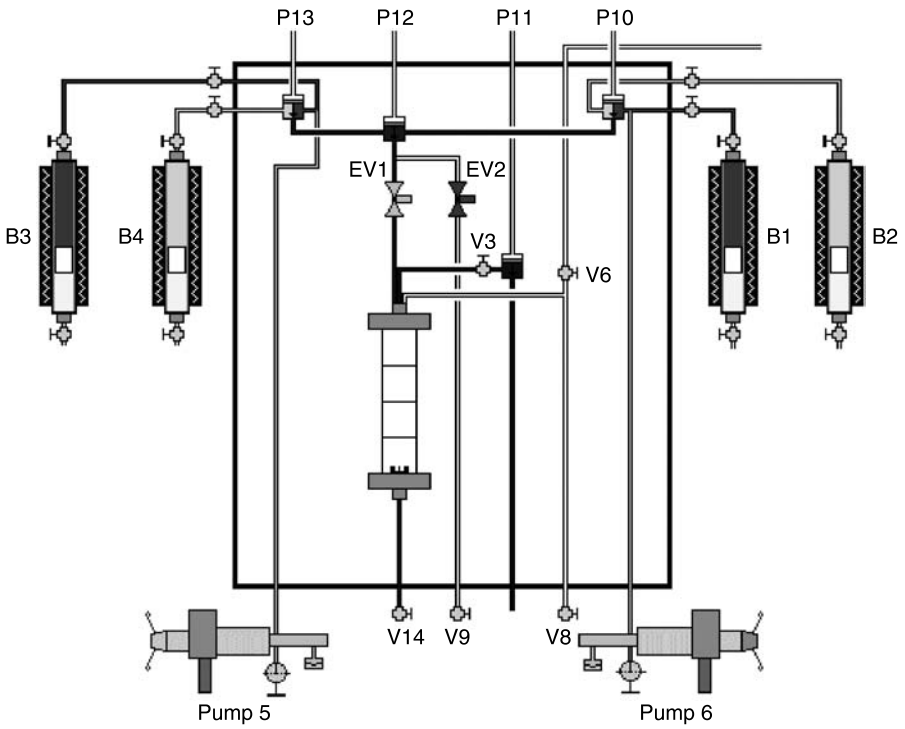

FIGURE 18.1 Schematic lay-out of high pressure separation rig.

The rig consists of four 600-cm^3 high-pressure sample cylinders, marked B1 to B4 in Figure 18.1. A selection of cylinders is filled with water or oil; with the aid of up to four independent motor driven high capacity piston pumps, the water and oils were pumped and mixed through choke valves. The pressure drop through the choke valves is backpressure controlled. The choke valve P12 is connected to the separation cell by a 50 cm 1/4" tube. The pressure in the separation cell is regulated by a backpressure-controlled valve (P11 in Figure 18.1). The separation cell is made of sapphire, assuring full visibility of the separation process. The maximum pressure in the cell is 200 bars. The cell is pressurized with natural gas to the experimental pressure before filling of the cell. Two pumps (5 and 6) were available for on-line chemicals injection. In the bottom of the cell there is a stirrer that is used at low rpm in order to give a small shear to the system during separation.

18.3.3 High-Pressure Video Microscopy

The video microscopy equipment is shown schematically in Figure 18.2. The system consists of a monochrome CCD camera (Pulnix TM-1300) with a Nikon 10X micro objective. A stroboscope (Polytec) with adjustable light intensity was used as light source. The stroboscope works by sending a brief, intense pulse of electric current through an inert gas, in this case xenon, which then emits a brilliant burst of white light. The stroboscope and the camera are synchronized so that while the camera is acquiring an image, the stroboscope emits a very short flash of bright

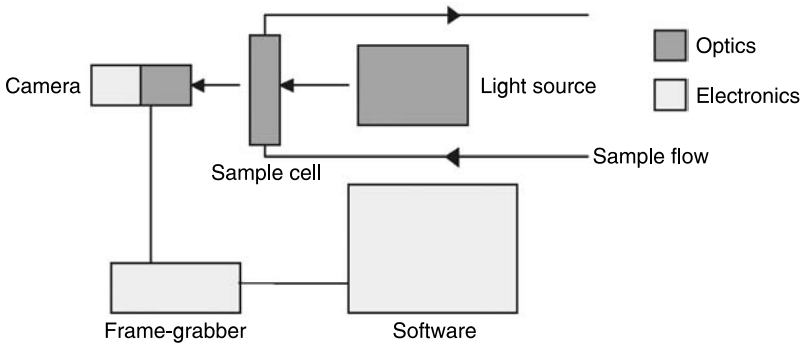

FIGURE 18.2 Schematic illustration of the high pressure video microscopy set-up.

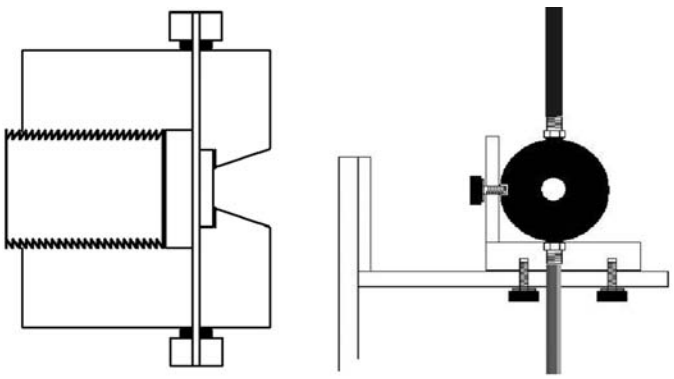

FIGURE 18.3 Sketch of high pressure cell and attachment.

light through the sample cell and the flowing emulsion. The effect on the grabbed images is that the droplets seem "frozen" in its movement.

The high pressure flow cell shown in Figure 18.3 was connected to the bottom outlet of the high pressure separation cell. The high pressure cell consists of a sapphire window in front and Plexiglas window in the rear. The cell was tested to withstand a pressure of 650 bars. A needle valve was placed after the high pressure flow cell, ensuring that the pressure in the flow cell was approximately the same as in the separation cell. Keeping the pressure constant in the separation cell and the flow cell is important as any release of dissolved gas from the dispersed oil droplets (due to pressure drop) would influence the oil droplet distribution. It would also be hard to distinguish between oil droplets and gas bubbles.

After a given separation time, the needle valve was opened and the separated water phase flowed through the video microscopy flow cell at a rate of approximately 1 to 2 ml/min. During this time an image series of 50 images was acquired. The video camera and the stroboscope were connected to a frame grabber PC card (Matrix Vision SDIG). The Image-Pro Plus version 4.2 (Media Cybernetics) software was used both for acquiring and analysis of the images. In order to obtain the correct droplet sizes, the image system was spatially calibrated using a graticule.

18.3.4 Image Analysis

The digital images were analyzed using the Image-Pro Plus software from Media Cybernetics, version 4.2. In-house Visual Basic macros for Image-Pro Plus made it possible to automatically process image series of 50 images instead of laborious single images analysis. Figure 18.4 shows the main steps in this analysis. First the images are enhanced by contrast, brightness, and sharpening adjustments [54]. Each image is built up of 640 × 480 pixels with a 256-value gray scale. By applying a threshold value to the image gray scale histogram (see Figure 18.5), the boundary of the droplets can be found. For each droplet a number of parameters are determined, like the diameter, area, roundness, aspect, and radius ratio. For a 50 image series, the number of droplets found varied from around 2000 to over 8000.

The images consist of pixels that are divided into a 256-value gray scale, where 0 is black and 255 is white. The droplets are darker than the background due to higher absorbance of light by the oil, and due to light scattering. In order to distinguish the droplets from the background, a threshold value is set on the basis of the gray scale pixel value characteristic for the droplets. Gray values less than the threshold is set to 0, while gray values greater or equal to the threshold is set to 255. In this way the gray scale image is converted to a binary image where the droplets are black and the background is white. All droplet measurements are then performed, but are of course influenced by the selected threshold value. Many image analysis programs include both manual threshold setting and automatic threshold routines. Selecting an overall threshold value for every image series only makes sense when experimental conditions are the same, like the

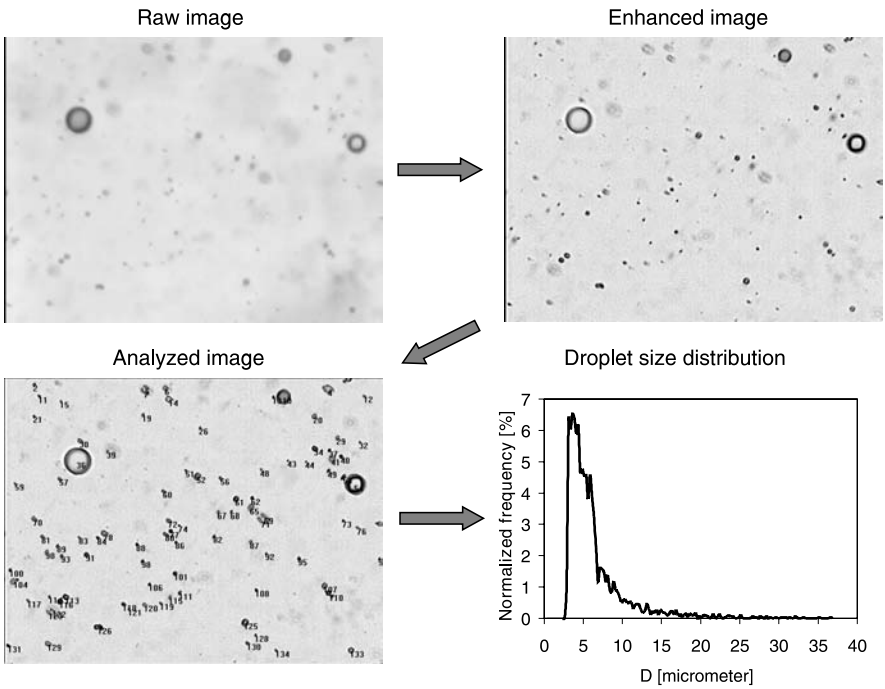

FIGURE 18.4 Image analysis. The details in the raw image are first enhanced, and then the boundary of the droplets is found by applying a threshold to the image gray scale histogram. The droplets are counted and droplet diameters are converted to droplet size distributions.

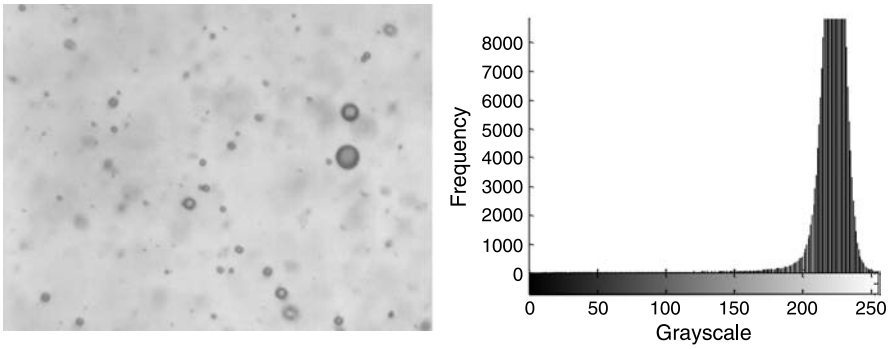

FIGURE 18.5 Image and its corresponding gray scale histogram.

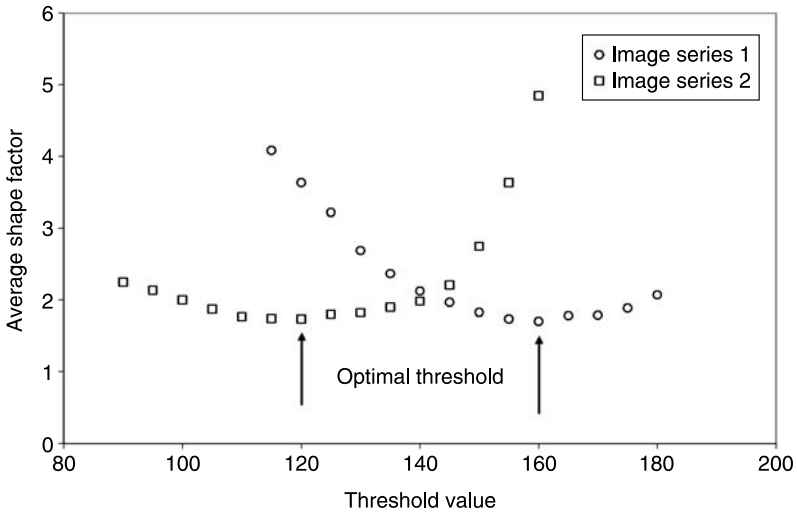

FIGURE 18.6 The average shape factor defined in Equation 18.6 as a function of the threshold for two image series. The two image series have different experimental settings for the intensity of the light source.

light source intensity, the focusing of the optics, and the overall optical density of the sample. The optical density will definitely change during the experiments as an oil-in-water emulsion containing many large oil droplets will absorb more light (and therefore the images will be darker) than an emulsion with few small droplets. It will also be difficult to obtain the same light intensity and focusing of optics during extended periods of time. All these concerns force one to have a method for setting the threshold.

One way to perform a test on the threshold value is to test how the average shape factor (defined in Equation 18.6) for all the droplets changes as one changes the threshold (see Figure 18.6). A threshold that is too high will add part of the background to the droplets and the average shape factor will increase. A threshold that is too low will only include a part of the droplets, and likewise the shape factor will increase. The optimal threshold value should then be the threshold value giving the global minimum for the average shape factor, as indicated in

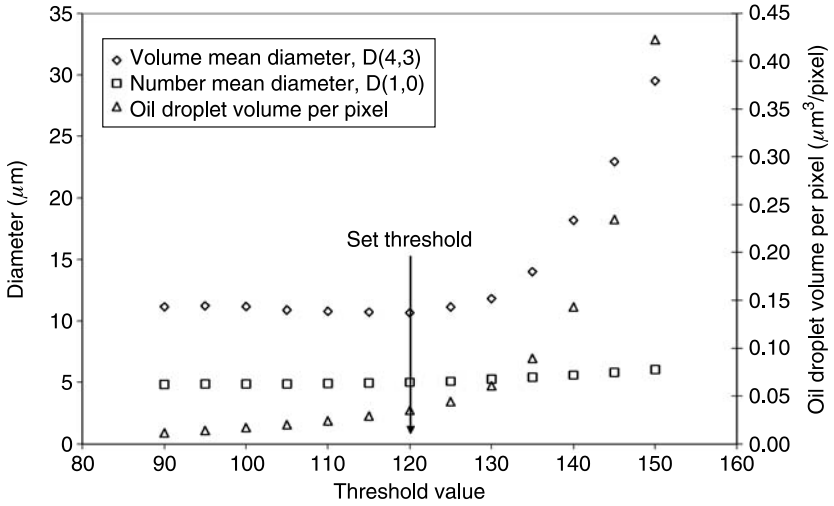

FIGURE 18.7 Effect of threshold on the mean diameter, volume diameter, and oil droplet volume per pixel.

Figure 18.6. Having a systematic method for determining the applied threshold value will also make the image analysis process operator independent.

The main droplet parameters we are interested in are the mean diameters (number and volume) and the oil droplet volume per pixel. The applied threshold value will influence all of these parameters. Figure 18.7 shows the effect of the threshold on the diameter values and the oil droplet volume. The mean diameter is more or less constant over the whole range; the volume mean diameter is constant at low threshold values, but increases rapidly at higher thresholds than the set optimal threshold. The oil droplet volume per pixel increases rapidly as we increase the threshold. Figure 18.7 illustrates the importance of having a systematic method for selecting the threshold value.

The threshold testing was performed using in-house macros developed for the Image-Pro Plus version 4.2 software from Media Cybernetics. Each series of 50 images were analyzed starting from a threshold of 90 to 180, increasing the threshold stepwise by 5. All the calculated droplet parameters were dumped to Excel (Microsoft) and the optimum threshold value was selected for a given image series. After finding the optimum threshold value, the different droplet sizes and volume were compared based on the experimental conditions in the high-pressure separation rig. In order to discriminate between spherical droplets and irregular shaped particles, all objects having a shape factor above 2.3 were rejected from the count. On average about 10% of the objects were removed in this process. The oil droplet volume per pixel is found from the summation of the volume of all droplets divided by the image resolution (640 × 480) and the number of images in each image series.

18.4 RESULTS

In the high pressure separation rig, oil and water are mixed through a choke valve and into the separation cell. The subsequent emulsion then starts to separate as oil droplets coalesce and cream upwards (for water continuous emulsions). Figure 18.8 shows a snapshot of the separation cell after a given separation time. Observing the height of the different phases (water, emulsion layer, oil, and foam) in the separation cell, a plot of the separation rate can be drawn (see Figure 18.9).

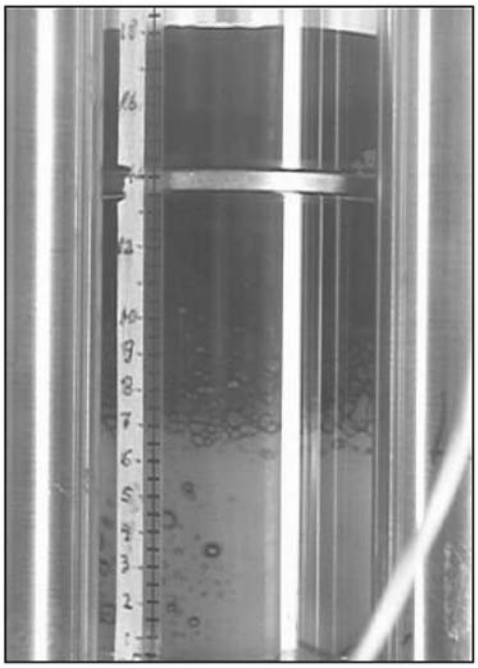

FIGURE 18.8 High pressure separation cell.

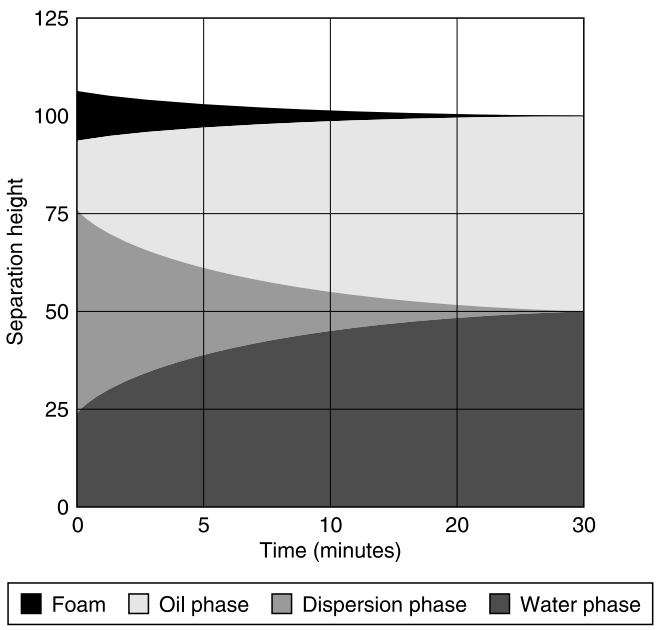

FIGURE 18.9 Separation curves.

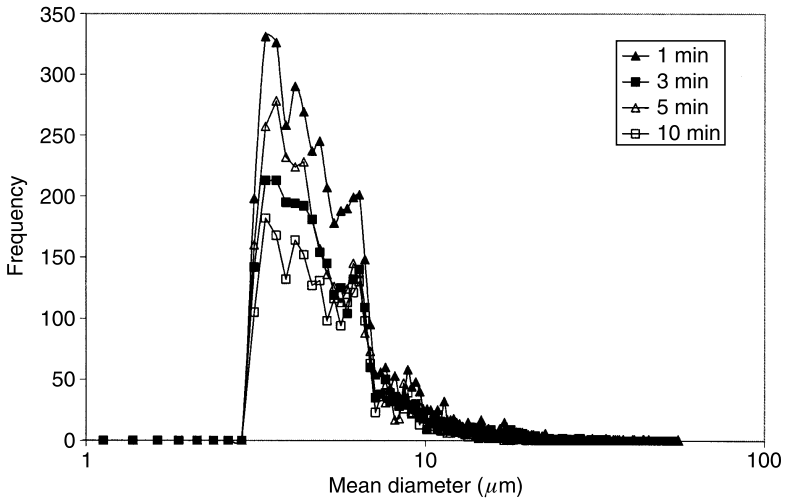

FIGURE 18.10 Mean droplet diameter frequency distributions of oil-in-water emulsions for varying retention time in the separation cell. Experimental conditions: T = 80 °C, pressure before choke valve: 65 bar, pressure drop over choke valve: 5 bar, water cut: 80%.

Both the amount of oil droplets and the droplet size distribution will change as the separation evolves.

Figure 18.10 shows the number distributions of the dispersed oil droplets in the water phase for a given system after 1, 3, 5, and 10 min of separation. The general trend is that the amount of droplets decreases with time, but there seems to be little change in the droplet size distributions. The mean diameter decreases from 6.6 μm after 1 min to 5.6 μm after 10 min. However, instead of looking at the frequency of the droplets and the mean diameter, we can look at how the volume of the oil-in-water phase is distributed across the different oil droplet sizes. Figure 18.11 shows the cumulative volume distributions at different separation times. The effect is much larger and it is much easier to see the trends. Looking at droplets larger than 30 μm, they account for 30% of the total oil volume after 1 min separation time. The amount decreases to around 12% after 1.5 min and to around 8% after 3 min. After 5 min separation time there are no droplets larger than 30 μm. This is all in accordance with Stokes' law [2], describing sedimentation and creaming processes.

Looking at the mean diameters, droplets with sizes up to around 6 μm do not account for more than between 10 and 20 vol% of the total oil droplet volume. In oil processing the main goal is to get the amount of water in export oil and oil in the produced water within certain limits. Too much water in the export oil reduces the price, while too much oil in the produced water implies regulations and/or fines from governmental authorities. In both cases the amount is based on weight percentages. This means that the correct droplet size distribution is not the number distribution but the volume distribution. Designing a separator based on the number distribution would lead to a much different result than if one used the volume distribution. The big difference between the number distribution and the volume distribution is due to the fact that as the diameter is increased by a factor of 1, the volume is increased by a factor of 3.

Figure 18.12 shows how the oil droplet volume per pixel decreases as the separation time increases. The change is largest in the beginning; the oil droplet volume is halved from 1 min

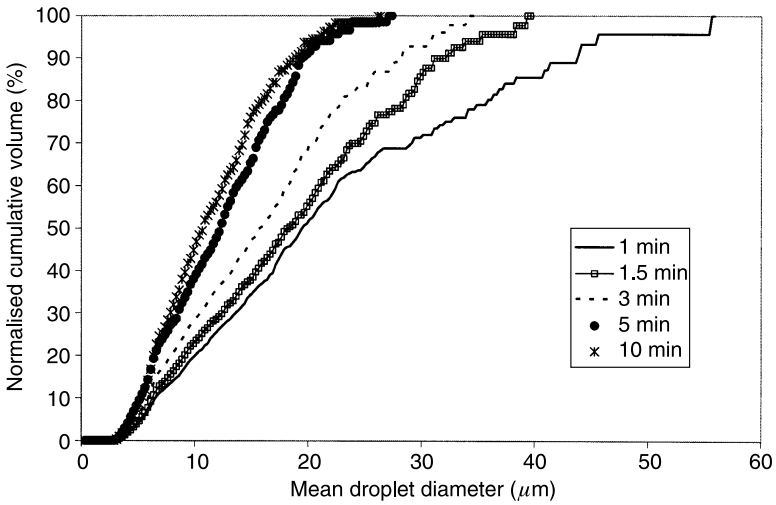

FIGURE 18.11 Cumulative volume distributions. Same experimental conditions as in Figure 18.10.

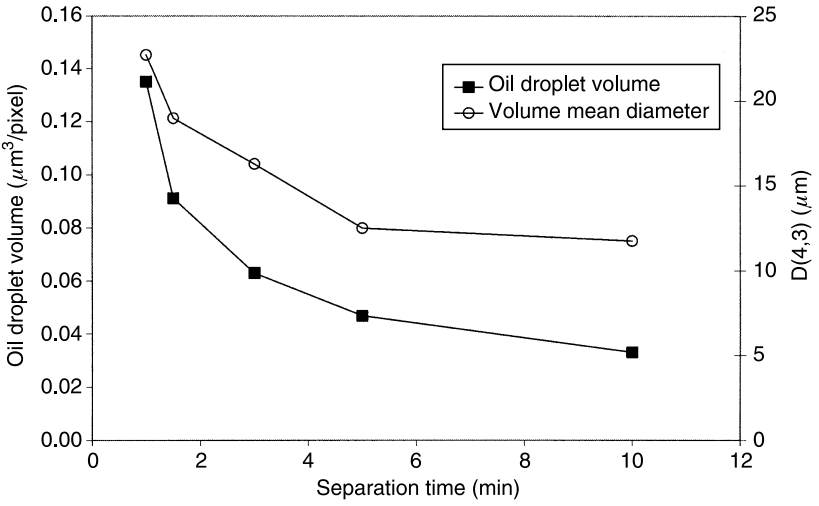

FIGURE 18.12 Changes in the oil droplet volume per pixel and the volume mean diameter, $D(4,3)$, as a function of the separation. Same experimental conditions as in Figure 18.10.

to 3 min separation time, while the next halving occurs after 10 min. For the volume mean diameter the same trend follows; it decreases rapidly in the beginning, while from 5 min to 10 min separation time, there is not much change. In the separation cell, there are two processes which affect the volume mean diameter. The creaming of the droplets removes the largest droplets, while flocculation and coalescence increases the droplet sizes. From Figure 18.12 one can qualitatively conclude that the creaming process is dominant in the beginning while the coalescence starts

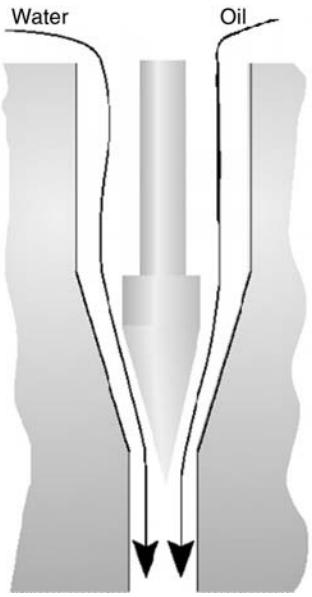

FIGURE 18.13 High pressure separation rig choke valve.

to be more and more important the longer the separation for the given system. Although some crude oil components, mainly small molecules like benzene, toluene, ethyl benzene, and xylene (BTEX) and low molecular weight phenols and naphthenic acids, will dissolve to some degree in the water phase, the oil droplet volume should be related to the total oil content in the water phase. In fact, the solubility of some of the higher molecular weight crude oil components are related to the amount of dispersed oil droplets in the water [55]. The video microscopy technique could therefore be applicable as an on-line measuring device for both droplet size distributions and for quality control of produced water at oil processing installations.

The amount of droplets and the droplet size distribution will also be influenced by factors like water cut and the pressure drop over the inlet choke valve. The pressure drop over the choke valve provides the shear forces necessary for the mixing of water and oil (see Figure 18.13). Increasing the pressure drop should increase the shear forces in the choke valve, leading to higher mixing of oil and water. On the other hand, increasing the pressure drop would also increase the release of gas, which in some cases could be positive for the phase separation, as the released gas bubbles can adsorb at the oil droplet surface and thereby increase the drag upwards. Increasing the pressure drop from 5 to 15 bars increases the amount of oil in the water phase (see Figure 18.14), due to the increased mixing in the choke valve. The effect is greater at 80% water cut, than for 95% water cut, for this particular system. Looking at the volume mean diameter in Figure 18.15, the increase in pressure drop gives an increase for $D(4,3)$ for 80% water cut, while there is no or little effect for 95% water cut.

The video microscopy is also capable of identifying inversion points for emulsions. Figure 18.16 shows how the amount of dispersed oil and the volume mean diameter of the oil droplets changes as we change the water cut for a given system. From the figure we can identify the following regions: at 50% water, the choke valve produces an oil continuous phase. Water sediments and only small oil droplets are drawn into the water phase. This leads to both

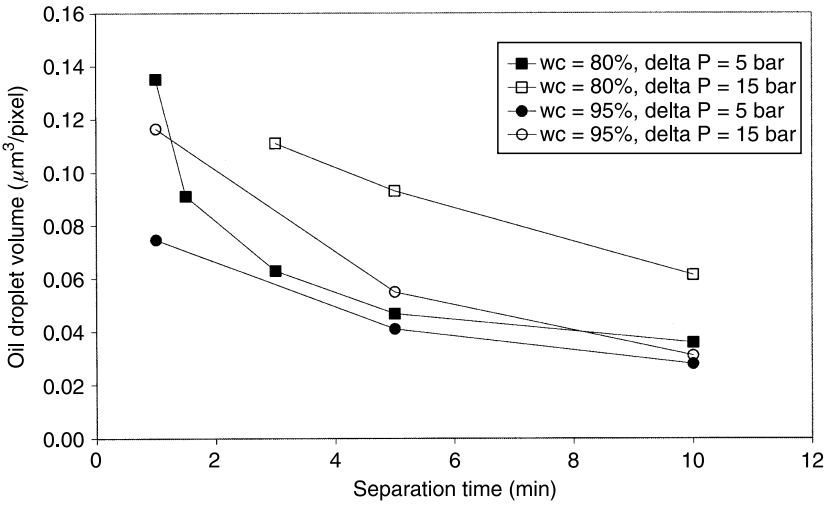

FIGURE 18.14 Effect of pressure drop on the oil droplet volume per pixel. Experimental conditions: T = 80 °C, pressure before choke valve: 65 bar.

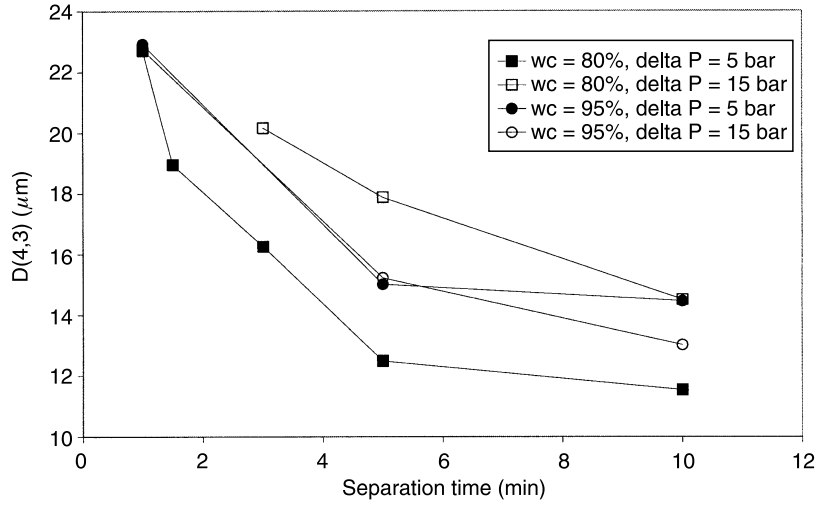

FIGURE 18.15 Effect of pressure drop on the volume mean diameter. Same experimental conditions as in Figure 18.14.

a low volume mean diameter and a low content of oil in the water phase. Moving to 80% water cut gives a huge increase in the oil content in the water phase, and the volume mean diameter is also increasing. At 80% water cut we have most likely a water continuous emulsion. We might also be close to the inversion point. At 95% water cut we have a water continuous emulsion and from 80% to 95% water cut we would expect a decrease in the amount of oil simply because we mix less oil into the water phase.

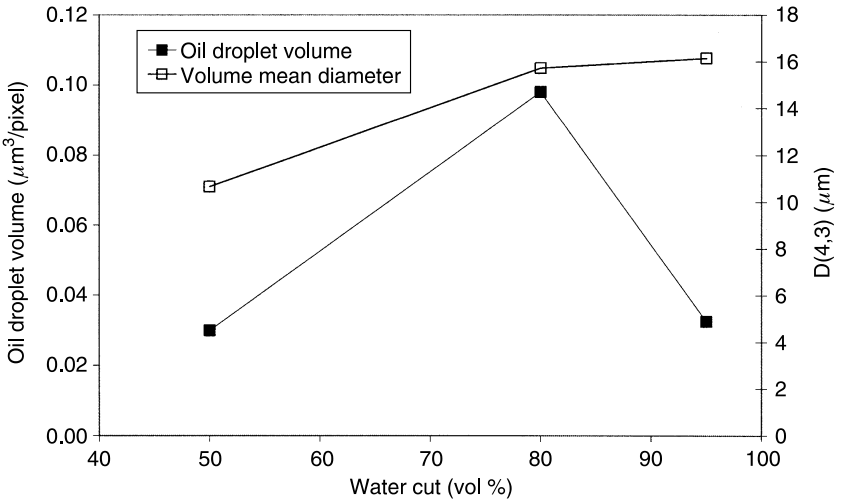

FIGURE 18.16 Effect of water cut. T = 65 °C, pressure before choke valve: 65 bar, pressure drop over choke valve: 5 bar.

18.5 CONCLUSIONS

A high pressure video microscopy system has been developed for measuring droplet sizes of dispersed oil droplets in oil-in-water emulsions under real conditions, that is, at high pressures and temperatures meeting the typical conditions for oil production facilities. A systematic method for selecting the threshold value for separating droplets from image background has been proposed. The method uses the average shape factor of the droplets as an indicator for the setting of the threshold. The video microscopy system is capable of detecting changes in the oil droplet size distribution and the changes in the amount of oil in the water phase due to effect of separation time, changes in the water cut, and changes in choke valve mixing. This system should be very attractive for online monitoring of the produced water quality.

ACKNOWLEDGMENTS

The support from the industrial members of the Ugelstad Laboratory at NTNU in Trondheim is acknowledged. Statoil ASA is acknowledged for the use of the high pressure separation equipment and the high pressure laboratory.

REFERENCES

1. Flanigan, D.A.; Stolhand, J.E.; Scribner, M.E.; Shimoda, E. Droplet Size Analysis: A New Tool for Improving Oilfield Separations. *63rd Ann. Tech. Conf. Exhib. Soc. Petr. Eng., Houston* **1988**, *SPE 18204*.
2. Geankoplis, C.J. *Transport Processes and Unit Operations*. Prentice Hall: New Jersey, 1983.
3. Cussler, E.L. *Diffusion. Mass Transfer in Fluid Systems. 2nd edition*. Cambridge University Press: Cambridge, 1997.
4. Jeelani, S.A.K.; Hartland, S. Effect of dispersion properties on the separation of batch liquid–liquid dispersions. *Ind. Eng. Chem. Res.* **1998**, *37*, 547–554.

5. Kumar, A.; Hartland, S. Gravity settling in liquid–liquid dispersions. *Can. J. Chem. Eng.* **1985**, *63*, 368–376.
6. Yu, G.Z.; Mao, Z.S. Sedimentation and coalescence profiles in liquid–liquid batch settling experiments. *Chem. Eng. Tech.* **2004**, *27*, 407–413.
7. Auflem, I.H.; Westvik, A.; Sjöblom, J. Destabilization of water-in-crude oil emulsions based on recombined oil samples at various pressures. *J. Dispers. Sci. Technol.* **2003**, *24*, 103–112.
8. Auflem, I.H.; Kallevik, H.; Westvik, A.; Sjöblom, J. Influence of pressure and solvency on the separation of water-in-crude-oil emulsions from the North Sea. *J. Petrol. Sci. Eng.* **2001**, *31*, 1–12.
9. Sjöblom, J.; Johnsen, E.E.; Westvik, A.; Ese, M.-H.; Djuve, J.; Auflem, I.H.; Kallevik, H. Demulsifiers in the Oil Industry. In *Encyclopedic Handbook of Emulsion Technology*. Sjöblom, J.; Ed.; Marcel Dekker: New York, 2001, pp 595–619.
10. Sæther, Ø. Video-enhanced Microscopy Investigation of Emulsion Droplets and Size Distributions. In *Encyclopedic Handbook of Emulsion Technology*. Sjöblom, J.; Ed.; Marcel Dekker: New York, 2001, pp 349–360.
11. Sjöblom, J.; Aske, N.; Auflem, I.H.; Brandal, Ø.; Havre, T.E.; Sæther, Ø.; Westvik, A.; Johnsen, E.E.; Kallevik, H. Our current understanding of water-in-crude oil emulsions. Recent characterization techniques and high pressure performance. *Adv. Colloid Interface Sci.* **2003**, *100*, 399–473.
12. Bhardwaj, A.; Hartland, S. Kinetics of coalescence of water droplets in water-in-crude oil-emulsions. *J. Dispers. Sci. Technol.* **1994**, *15*, 133–146.
13. Mason, S.L.; May, K.; Hartland, S. Drop size and concentration profile determination in petroleum emulsion separation. *Colloid Surf. A* **1995**, *96*, 85–92.
14. Holt, Ø.; Sæther, Ø.; Sjöblom, J.; Dukhin, S.S.; Mishchuk, N.A. Video enhanced microscopic investigation of reversible Brownian coagulation in dilute oil-in-water emulsions. *Colloid Surf. A* **1997**, *123*, 195–207.
15. Holt, Ø.; Sæther, Ø.; Sjöblom, J.; Dukhin, S.S.; Mishchuk, N.A. Investigation of reversible Brownian flocculation and intradoublet coalescence in o/w emulsions by means of video enhanced microscopy. *Colloid Surf. A* **1998**, *141*, 269–278.
16. Jokela, P.; Fletcher, P.D.I.; Aveyard, R.; Lu, J.R. The use of computerized microscopic image-analysis to determine emulsion droplet size distributions. *J. Colloid Interface Sci.* **1990**, *134*, 417–426.
17. Mishchuk, N.A.; Verbich, S.V.; Dukhin, S.S.; Holt, Ø.; Sjöblom, J. Rapid Brownian coagulation in dilute polydisperse emulsions. *J. Dispers. Sci. Technol.* **1997**, *18*, 517–537.
18. Pacek, A.W.; Moore, I.P.T.; Calabrese, R.V.; Nienow, A.W. Evolution of drop size distributions and average drop diameter in liquid–liquid dispersions before and after phase inversion. *Chem. Eng. Res. & Des.* **1993**, *71*, 340–341.
19. Pacek, A.W.; Moore, I.P.T.; Nienow, A.W.; Calabrese, R.V. Video technique for measuring dynamics of liquid–liquid dispersion during phase inversion. *Aiche J.* **1994**, *40*, 1940–1949.
20. Pacek, A.W.; Nienow, A.W. Measurement of drop size distribution in concentrated liquid–liquid dispersions – video and capillary techniques. *Chem. Eng. Res. & Des.* **1995**, *73*, 512–518.
21. Pacek, A.W.; Nienow, A.W.; Moore, I.P.T. On the structure of turbulent liquid–liquid dispersed flows in an agitated vessel. *Chem. Eng. Sci.* **1994**, *49*, 3485–3498.
22. Sæther, Ø.; Sjöblom, J.; Verbich, S.V.; Mishchuk, N.A.; Dukhin, S.S. Video-microscopic investigation of the coupling of reversible flocculation and coalescence. *Colloid Surf. A* **1998**, *142*, 189–200.
23. Sæther, Ø.; Dukhin, S.S.; Sjöblom, J.; Holt, Ø. The lifetime of a doublet of miniemulsion droplets and its measurement with the use of video microscopy. *Colloid J.* **1995**, *57*, 793–799.
24. Wang, Y.Y.; Bian, S.Z.; Wu, D. A simplified method for measuring dilute emulsion stability. *Pestic. Sci.* **1995**, *44*, 201–203.
25. Lashmar, U.T.; Richardson, J.P.; Erbod, A. Correlation of physical parameters of an oil-in-water emulsion with manufacturing procedures and stability. *Int. J. Pharm.* **1995**, *125*, 315–325.
26. Pather, S.I.; Neau, S.H.; Pather, S. A comparison of 2 quality assessment methods for emulsions. *J. Pharm. Biomed. Anal.* **1995**, *13*, 1283–1289.

27. Kamel, A.H.; Akashah, S.A.; Leeri, F.A.; Fahim, M.A. Particle-size distribution in oil–water dispersions using image-processing. *Comp. & Chem. Eng.* **1987**, *11*, 435–439.
28. Hazlett, R.D.; Schechter, R.S.; Aggarwal, J.K. Image-processing techniques for the estimation of drop size distributions. *Ind. Eng. Chem. Fundam.* **1985**, *24*, 101–105.
29. Scott, T.C.; Sisson, W.G. Droplet size characteristics and energy input requirements of emulsions formed using high-intensity-pulsed electric-fields. *Sep. Sci. Tech.* **1988**, *23*, 1541–1550.
30. Yan, Y.D.; Clarke, J.H.R. Insitu determination of particle-size distributions in colloids. *Adv. Colloid Interface Sci.* **1989**, *29*, 277–318.
31. Glatter, O.; Hofer, M. Interpretation of elastic light-scattering data. 3. Determination of size distributions of polydisperse systems. *J. Colloid Interface Sci.* **1988**, *122*, 496–506.
32. Lindner, H.; Fritz, G.; Glatter, O. Measurements on concentrated oil in water emulsions using static light scattering. *J. Colloid Interface Sci.* **2001**, *242*, 239–246.
33. Washington, C.; Sizer, T. Stability of tpn mixtures compounded from lipofundin-s and aminoplex amino-acid solutions – comparison of laser diffraction and coulter-counter droplet size analysis. *Int. J. Pharm.* **1992**, *83*, 227–231.
34. Eberth, K.; Merry, J. A comparative-study of emulsions prepared by ultrasound and by a conventional method – droplet size measurements by means of a coulter-counter and microscopy. *Int. J. Pharm.* **1983**, *14*, 349–353.
35. Sontum, P.C.; Kolderup, E.M.; Veldt, D.I. Coulter counting and light diffraction analysis applied to characterisation of oil–water emulsions. *J. Pharm. Biomed. Anal.* **1997**, *15*, 1641–1646.
36. Yan, Y.D.; Clarke, J.H.R. Dynamic light-scattering from concentrated water-in-oil microemulsions: The coupling of optical and size polydispersity. *J. Chem. Phys.* **1990**, *93*, 4501–4509.
37. Finsy, R. Particle sizing by quasi-elastic light-scattering. *Adv. Colloid Interface Sci.* **1994**, *52*, 79–143.
38. Crawley, G.; Cournil, M.; DiBenedetto, D. Size analysis of fine particle suspensions by spectral turbidimetry: Potential and limits. *Powder Technol.* **1997**, *91*, 197–208.
39. Raphael, M.; Rohani, S. On-line estimation of solids concentrations and mean particle size using a turbidimetry method. *Powder Technol.* **1996**, *89*, 157–163.
40. Li, M.Z.; Wilkinson, D. Particle size distribution determination from spectral extinction using evolutionary programming. *Chem. Eng. Sci.* **2001**, *56*, 3045–3052.
41. Roland, I.; Piel, G.; Delattre, L.; Evrard, B. Systematic characterization of oil-in-water emulsions for formulation design. *Int. J. Pharm.* **2003**, *263*, 85–94.
42. Balinov, B.; Urdahl, O.; Söderman, O.; Sjöblom, J. Characterization of water-in-crude-oil emulsions by the NMR self-diffusion technique. *Colloid Surf. A* **1994**, *82*, 173–181.
43. Balinov, B.; Soderman, O.; Warnheim, T. Determination of water droplet size in margarines and low-calorie spreads by nuclear-magnetic-resonance self-diffusion. *J. Am. Oil Chem. Soc.* **1994**, *71*, 513–518.
44. Hollingsworth, K.G.; Sederman, A.J.; Buckley, C.; Gladden, L.F.; Johns, M.L. Fast emulsion droplet sizing using NMR self-diffusion measurements. *J. Colloid Interface Sci.* **2004**, *274*, 244–250.
45. Vandenenden, J.C.; Waddington, D.; Vanaalst, H.; Vankralingen, C.G.; Packer, K.J. Rapid-determination of water droplet size distributions by pfg-nmr. *J. Colloid Interface Sci.* **1990**, *140*, 105–113.
46. Packer, K.J.; Rees, C. Pulsed nmr studies of restricted diffusion. 1. Droplet size distributions in emulsions. *J. Colloid Interface Sci.* **1972**, *40*, 206.
47. Li, X.Y.; Cox, J.C.; Flumerfelt, R.W. Determination of emulsion size distribution by NMR restricted diffusion measurement. *AICHE J.* **1992**, *38*, 1671–1674.
48. Alba, F.; Crawley, G.M.; Fatkin, J.; Higgs, D.M.J.; Kippax, P.G. Acoustic spectroscopy as a technique for the particle sizing of high concentration colloids, emulsions and suspensions. *Colloid Surf. A* **1999**, *153*, 495–502.
49. Haskell, R.J. Characterization of submicron systems via optical methods. *J. Pharm. Sci.* **1998**, *87*, 125–129.
50. Goodwin, J. *Colloids and Interfaces with Surfactants and Polymers*. Wiley: Chichester, UK, 2004.
51. Murphy, D.B. *Fundamentals of Light Microscopy and Electronic Imaging*. Wiley-Liss: New York, 2001.

52. Jillavenkatesa, A.; Dapkunas, S.J.; Lum, L.-S.H. In *Particle Size Characterization*. National Institute of Standards and Technology, 2001; Special Publication.
53. Allen, T. *Particle Size Measurement. Volume 1. Powder Sampling and Particle Size Measurement*. Chapman & Hall: London, 1997.
54. Russ, J.C. *The Image Processing Handbook, 4th Edition*. CRC Press: Boca Raton, 2002.
55. Grini, P.G.; Hjelsvold, M.; Johnson, S. Choosing Produced Water Treatment Technologies Based on Environmental Impact Reduction. *Paper presented at SPE International Conference on Health, Safety and Environment in Oil and Gas Exploration and Production, Kuala Lumpur, Malaysia* **2002**, *SPE 74002*.